

● *Original Contribution*

DIRECT STRAIN ESTIMATION IN ELASTOGRAPHY USING SPECTRAL CROSS-CORRELATION

T. VARGHESE,* E. E. KONOFAGOU,* J. OPHIR,* S. K. ALAM* and M. BILGEN†

*Ultrasonics Laboratory, †MRI Laboratory, Department of Radiology, The University of Texas Medical School, Houston, TX, USA

(Received 7 April 2000; in final form 30 August 2000)

Abstract—Spectral estimation of tissue strain has been performed previously by using the centroid shift of the power spectrum or by estimating the variation in the mean scatterer spacing in the spectral domain. The centroid shift method illustrates the robustness of the direct, incoherent strain estimator. In this paper, we present a strain estimator that uses spectral cross-correlation of the pre- and postcompression power spectrum. The centroid shift estimator estimates strain from the mean center frequency shift, while the spectral cross-correlation estimates the shift over the entire spectrum. Spectral cross-correlation is shown to be more sensitive to small shifts in the power spectrum and, thus, provides better estimation for smaller strains when compared to the spectral centroid shift. Spectral cross-correlation shares all the advantages gained using the spectral centroid shift, in addition to providing accurate and precise strain estimation for small strains. The variance and noise properties of the spectral strain estimators quantified by their respective strain filters are also presented. © 2001 World Federation for Ultrasound in Medicine & Biology.

Key Words: Centroid, Cross-correlation, Elastography, Elastogram, Imaging, Strain, Spectral shift, Strain filter, Ultrasound.

INTRODUCTION

Imaging tissue elastic parameters for diagnosis of disease is rapidly drawing attention for its ability to provide noninvasive and *in vivo* new information on biological tissue (Wilson and Robinson 1982; Krouskop et al. 1987; Yamakoshi et al. 1990; Parker et al. 1990; Ophir et al. 1991, 1997; O'Donnell et al. 1994; Talhami et al. 1994). Currently, the estimators used for strain estimation can be classified into either coherent or incoherent estimation techniques. Coherent techniques include time-domain cross-correlation (Ophir et al. 1991; Céspedes 1993), and a Fourier-based speckle phase-tracking technique (O'Donnell et al. 1991). On the other hand, a number of incoherent estimators have also been described in the literature, such as optical flow-based speckle tracking (Bertrand et al. 1989), envelope cross-correlation

(Varghese and Ophir 1998), spectral centroid shift (Varghese et al. 1999; Konofagou et al. 1999), and using the variation in the mean-scatterer spacing (Talhami et al. 1994).

All spectral approaches (Varghese et al. 1999; Konofagou et al. 1999; Talhami et al. 1994), are based on the Fourier scaling property that converts strain into a spectral shift (Fig. 1). Estimation of the spectral shift from the power spectrum of the pre- and postcompression signals, leads to a robust (noise resistant) and motion invariant method (Konofagou et al. 1999) of estimating strain. The spectral shift of the postcompression power spectrum can be estimated by directly computing the shift in the power spectrum or by estimating scatterer parameters that are affected by the applied strain for, for example, the mean scatterer spacing (Fellingham and Sommer 1984; Kuc et al. 1986; Landini and Verrazzanni 1990; Varghese and Donohue 1994, 1995; Varghese 1995). The technique proposed by Talhami et al. (1994) uses the second approach, which estimates the change in the mean scatterer spacing with the applied strain and, therefore, depends on the presence of underlying tissue periodicities in the scatterer structure. The ratio of the standard deviation of the scatterer spacing (difference in

Dr. Konofagou's present address is Brigham and Women's Hospital, Harvard Medical School, Boston, MA-02115, USA. Dr. Alam's present address is Riverside Research Institute, New York, NY 10036 USA.

Address correspondence to: Dr. Tomy Varghese, Department of Medical Physics, Rm 1530, University of Madison-Wisconsin, 1300 University Avenue, Madison, WI 53706, USA. E-mail: tvarghese@facstaff.wisc.edu

the mean scatterer spacing before and after tissue compression) to the mean scatterer spacing before compression is used to estimate strain (Talhami et al. 1994).

Strain in traditional elastography is estimated from the gradient of the displacement estimate (Ophir et al. 1991). However, the gradient operation introduces additional noise amplification into the strain estimation process. The spectral cross-correlation strain estimator, like the spectral centroid shift (Konofagou et al. 1999) and the adaptive strain estimator (Alam et al. 1998), provides direct estimates of the strain and avoids the use of a gradient operation. The centroid shift estimator relies on the estimate of mean center frequency shift with strain, but the spectral cross-correlation estimator presented in this paper estimates the shift over the entire power spectrum.

Spectral estimation of tissue strains using the centroid shift (Konofagou et al. 1999) has been shown to produce quality elastograms for large applied strains. However, the robustness and noise performance of these estimators have yet to be quantified in terms of the strain estimation variance and strain filter (SF) analysis (Varghese and Ophir 1997; Varghese et al. 1998). Theoretical expressions for the variance for both the spectral estimators (*i.e.*, spectral centroid shift and spectral cross-correlation) are derived in this paper.

The power spectrum for the spectral methods can be generated either by time-averaging (Welch 1967; Varghese 1995; Varghese and Donohue 1994) the Fourier spectra obtained from an ensemble of A-lines or by frequency smoothing (Varghese 1995; Varghese and Donohue 1995) (*i.e.*, a moving average of the complex Fourier spectra obtained from a single data segment). The results illustrate that the variance of the spectral strain estimators depends more strongly on the length of the windowed data segment used to obtain the power spectrum than on the number of averages of the Fourier spectra or the length of the frequency smoothing window. In general, the variance reduces with an increase in the windowed data segment, which, however, contributes to a loss in resolution. The spectral resolution depends on the window length used in strain estimation and the length of the frequency-smoothing window. The resolution of the strain estimate depends only on the length of the strain estimation window, when compared to the time-domain cross-correlation, where the resolution depends on the strain estimation window and the overlap between the data segments (Alam et al. 2000). In either case, the resolution of any convolution-based imaging system such as ultrasonic imaging is ultimately diffraction-limited.

The underlying theory of the spectral cross-correlation strain estimator, along with the variance analysis and noise characterization of the spectral methods, is pre-

sented in the next section. Simulation results that corroborate the theoretical results are presented in the following section. Simulated and experimental elastograms provide a qualitative comparison of the noise performance of the coherent and incoherent strain estimators. The contributions of this paper are discussed and summarized in the Conclusion section.

THEORY

Signal and noise model

The pre- and postcompression echo signals are given as follows (Céspedes 1993; Bilgen and Insana 1996; Varghese et al. 1998):

$$r_1(z) = h(z)*e(z) + n_1(z) \quad (1)$$

$$r_2(z) = h(z)*e(az) + n_2(z), \quad (2)$$

where z is a spatial variable, $r_1(z)$ and $r_2(z)$ are the backscattered RF signals before and after compression, respectively, $h(z)$ is the impulse response of the US system or point-spread function (PSF), $e(z)$ is the scattering function, $n_1(z)$ and $n_2(z)$ are independent zero mean white noise sources and a is the compression coefficient (or strain factor) linked to strain s through (Céspedes 1993; Bilgen and Insana 1996):

$$a = \frac{1}{1-s} \approx 1 + s. \quad (3)$$

Assuming Gaussian-modulated sine and cosine pulses for both the US PSF and the scattering function, we have (Insana et al. 1990; Lizzi et al. 1987; Varghese et al. 1998):

$$h(z) = \frac{1}{\sqrt{2\pi}L_h} \exp(-z^2/2L_h^2) \sin(k_h z) \quad (4)$$

and

$$e(z) = \frac{1}{\sqrt{2\pi}L_e} \exp(-z^2/2L_e^2) \cos(k_e z), \quad (5)$$

where L_h and L_e are the bandwidths of the PSF and of the scattering function, respectively, k_h is the spatial center frequency of the PSF and k_e is the spatial frequency of the scattering function. The power spectra of the pre- and postcompression RF signals (we only consider the positive frequency) are given, respectively, by:

$$\begin{aligned}
R_1(k) &= \frac{1}{4} \exp\left(-\frac{1}{2} [(k - k_h)^2 L_h^2 + (k - k_e)^2 L_e^2]\right) \\
&\quad + N_1(k) \\
R_2(k) &= \frac{1}{4a} \exp\left(-\frac{1}{2} \left[(k - k_h)^2 L_h^2 + (k - ak_e)^2 \frac{L_e^2}{a^2}\right]\right) \\
&\quad + N_2(k), \quad (6)
\end{aligned}$$

where $n_1(z)$ and $n_2(z)$ are independent zero mean white noise processes, *i.e.*,

$$\langle N_1(k) \rangle = \langle N_2(k) \rangle = 0.$$

The subscripts ₁ and ₂ denote pre- and postcompression parameters, respectively, throughout this paper.

Strain estimation using spectral cross-correlation

The spectral cross-correlation algorithm relies on the estimation of the spectral shift over the entire pre- and postcompression power spectra using the cross-correlation algorithm. The cross-correlation function between the pre- and the postcompression power spectra illustrated in eqn. (6) is given by:

$$S(k_0) = \int_{-\infty}^{\infty} R_1(k + k_0) R_2(k) dk, \quad (7)$$

where k_0 denotes the spectral shift. The expression for the spectral shift using spectral cross-correlation, eqn (7), is derived in Appendix A, and is given by:

$$k_0 \approx -\frac{k_h}{2} s, \quad (8)$$

where k_h is the center frequency of the PSF, and s is the applied strain. The spectral shift in the pre- and postcompression power spectrum, therefore, provides a direct estimate of tissue strain as illustrated in eqn (8). The tissue strain scaled by the center frequency of the PSF determines the spectral shift.

Variance of the spectral cross-correlation strain estimator

The variance for the spectral cross-correlation method is derived under the assumption that the power spectrum of a signal can be modeled as a Gaussian function (for simplification in the analysis). The Cramér–Rao lower bound (CRLB) on the variance of the displacement (or spectral shift) estimator for a Gaussian envelope ($\sigma^2(\hat{s})_{\text{CRLB},\rho}$) has been previously derived

(Weinstein and Weiss 1984; Walker and Trahey 1995; Varghese and Ophir 1998), and is given by:

$$\sigma^2(\hat{s})_{\text{CRLB},\rho} \geq \frac{3c}{2\pi^2 Z B^3} \left[\frac{1}{\rho^2} \left(1 + \frac{1}{\text{SNR}_s^2} \right)^2 - 1 \right], \quad (9)$$

where ρ is the correlation coefficient between the pre- and postcompression signals, SNR_s is the sonographic SNR, Z is the length of the windowed data segment, B is the bandwidth of the power spectrum and c represents the speed of sound. This expression predicts the lower bound on the jitter errors incurred while estimating the displacement between two partially correlated envelope signals corrupted by decorrelation and electronic noise. The correlation coefficient used in eqn (9) varies with applied strain and is, itself, also dependent on the window length used to compute the normalized cross-correlation function. An expression for the spectral correlation coefficient that depends on tissue strain, axial signal decorrelation and the finite length window is derived in Appendix B.

Because we use the power spectrum to estimate the spectral shift, the variance of the power spectral estimates themselves must be considered. The CRLB on the variance of the power spectral estimate ($\sigma_{\text{PSD}}^2(\cdot)_{\text{CRLB}}$) is derived in Appendix C, eqn (C-3), and is given by:

$$\sigma_{\text{PSD}}^2(\cdot)_{\text{CRLB}} \geq \frac{1}{\frac{Z}{2} \int_{-1/2}^{1/2} \left(\frac{k(L_h^2 + L_e^2) R(k)}{R(k) + 1/\text{SNR}_c^2} \right)^2 dk} \quad (10)$$

where Z is the data window length and L_h and L_e are the bandwidths of the PSF and scatterer function. The CRLB bound on the variance of the spectral cross-correlation estimator ($\sigma^2(\hat{s})_{\text{SCC}}$), therefore, is given by:

$$\sigma^2(\hat{s})_{\text{SCC}} \geq \sigma^2(\hat{s})_{\text{CRLB},\rho} + \sigma_{\text{PSD}}^2(\cdot)_{\text{CRLB}}. \quad (11)$$

Knowledge of the variance of the spectral cross-correlation strain estimator can be used to obtain the SF, as discussed in the next section. The CRLB bound on the variance of the spectral centroid shift strain estimator is derived in Appendix D.

THEORETICAL RESULTS

Varghese and Ophir (1997) proposed a general theoretical framework known as the strain filter (SF) that characterizes the noise properties of the elastographic system. The SF describes the relationship among the

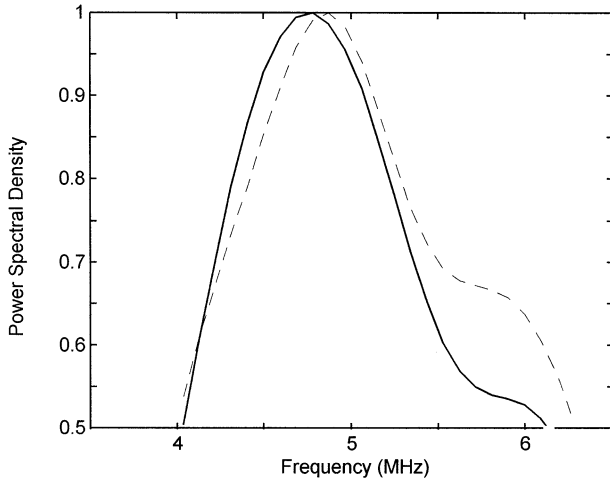


Fig. 1. The spectral shift in the power spectrum due to a 0.5% strain. Note that the peak of the spectrum is upshifted by the amount of strain incurred. This figure was obtained using simulated RF pre- and postcompression signals using the following parameters $Z = 3$ mm; $B = 60\%$; $k_o = k_f = 20.4$ mm⁻¹ (5-MHz center frequency).

resolution, dynamic range (DR_e), sensitivity (S_{\min}) and elastographic SNR (SNR_e), and may be plotted as a graph of the upper bound of the SNR_e vs. the strain experienced by the tissue. The upper bound of the SNR_e is obtained when the tissue strain (s) and the tightest lower bound on the strain estimation standard deviation ($\sigma(s)_{ZZLB,\rho}$ ¹ the modified Ziv-Zakai lower bound) is used to compute the SNR_e :

$$SNR_e^{UB} = \frac{s}{\sigma(s)_{ZZLB,\rho}}. \quad (12)$$

For the spectral cross-correlation strain estimator, we use the ZZLB derived for time-delay estimation (TDE) with envelope signals (Weinstein and Weiss 1984), and similar to the treatment for strain estimation (Varghese and Ophir 1998). Because spectral cross-correlation essentially estimates the displacement or spectral shift between the pre- and postcompression power spectra, the ZZLB expression derived by Weinstein and Weiss (1984) applies to the spectral situation with the appropriate change of variables. Incorporating the modified ZZLB expression for the TDE variance for envelope signals from the treatment of Weinstein and Weiss, we obtain:

¹ The lower bounds on the strain estimation variance are denoted with an additional subscript ρ to indicate that these variances are computed for partially correlated signals. These lower bounds converge to the classical bounds when $\rho = 1$.

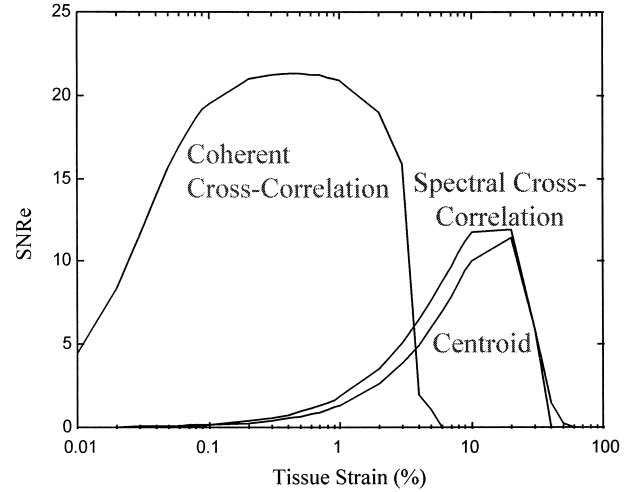


Fig. 2. Comparison of the strain estimation using cross-correlation vs. the spectral strain estimators using the theoretical SFs. The SFs were obtained using the following parameters: $Z = 3$ mm; $B = 60\%$; $k_o = k_f = 20.4$ mm⁻¹ (5-MHz center frequency).

$$\sigma^2(s)_{ZZLB,\rho} \geq \begin{cases} (sZ)^2/12 (2BZ/c)SNR_c < \psi \\ \text{Threshold } \psi < (2BZ/c)SNR_c < \beta, \\ \sigma^2(\delta)_{CRLB,\rho} \beta < (2BZ/c)SNR_c \end{cases} \quad (13)$$

where β and ψ are the threshold points presented in Weinstein and Weiss (1984), and SNR_c is the composite SNR (Varghese and Ophir 1997). Equation (13) illustrates the two distinct operating regions for $\sigma^2(s)_{ZZLB,\rho}$, depending on the value of $(2BZ/c)SNR_c$. A distinct threshold region is observed between the CRLB and the constant variance level. The variance increases exponentially in this threshold region (Weinstein and Weiss 1984). Accurate estimation of the strain is possible only within the CRLB.

Figure 2 presents a comparison of the SFs obtained using the spectral cross-correlation and centroid shift methods and the time-domain coherent cross-correlation method. The SFs are obtained using the following parameters: $Z = 3$ mm, $SNR_s = 40$ dB, $B = 60\%$, $k_o = k_f = 20.4$ mm⁻¹ (5-MHz center frequency), unless otherwise specified. Observe that, as expected, the coherent cross-correlation method performs better for low strains, and the spectral methods provide better performance at large applied strains. Both the centroid shift and the spectral cross-correlation strain estimator provide similar noise performance; however, spectral cross-correlation provides better sensitivity and has the higher SNR_e value. Note also the reduction in the SNR_e and dynamic range between the coherent cross-correlation and spectral methods.

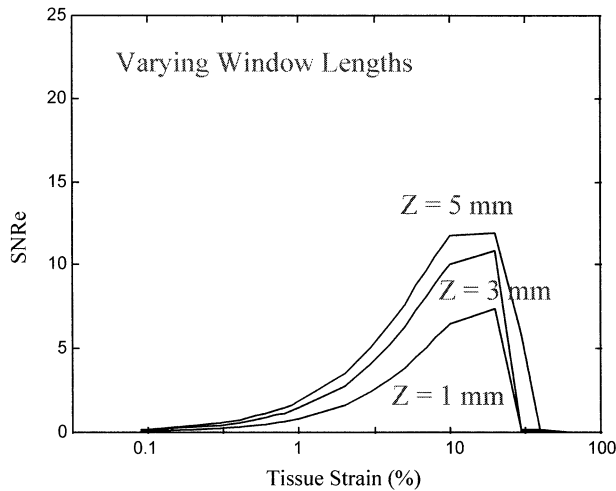


Fig. 3. A group of three spectral SFs corresponding to window lengths of 1 mm, 3 mm and 5 mm, respectively. The strain filters were obtained using the following parameters: $B = 60\%$; $k_o = k_f = 20.4 \text{ mm}^{-1}$. Note the improvement in the sensitivity, saturation and maximum SNR_e value with an increase in the window length.

The variation in the spectral cross-correlation SFs for different window lengths is illustrated in Fig. 3. Note that most of the elastographic quality parameters, such as the sensitivity, saturation, dynamic range and SNR_e (Varghese *et al.* 1998), other than the resolution, improve with the use of larger window lengths. This improvement is due to reduced variance of the power spectral estimate with the use of larger window lengths. In a similar manner, the variation in the SFs for different center frequencies (with a fixed fractional bandwidth of 60%) is illustrated in Fig. 4. Here, the noise performance is similar to that exhibited by the coherent cross-correlation strain estimator (Varghese and Ophir 1997; Varghese *et al.* 1998), where the sensitivity and the maximum SNR_e value improve with an increase in the center frequency; however, the saturation value or the maximum value of the strain estimated reduces. The theoretical spectral SFs are obtained assuming an unbiased strain estimate; however, the spectral strain estimates have a bias, see eqn (8). This bias in the spectral strain estimate overestimates the value of the theoretical elastographic signal-to-noise ratio (SNR_e).

In this section, we presented the theoretical evaluation of the variance of the spectral strain estimators along with their corresponding SFs. The theoretical results are corroborated using simulation results in the following section.

SIMULATION RESULTS

Methods

The pre- and postcompression RF signals are simulated for a 30-mm segment with a 48-MHz sampling

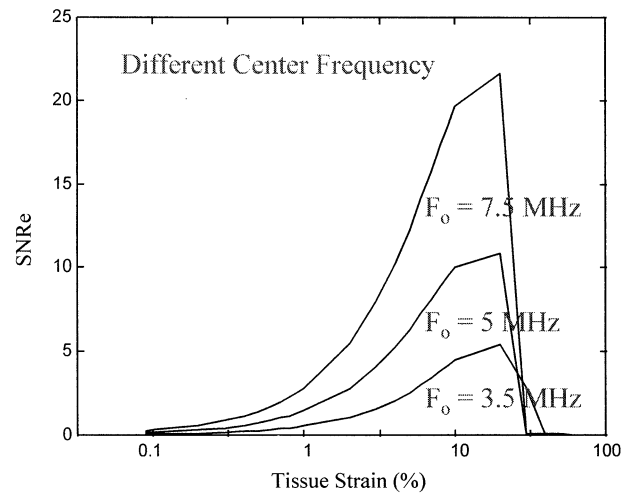


Fig. 4. A group of three spectral SFs corresponding to center frequencies of 3.5, 5 and 7.5 MHz, respectively. The strain filters were obtained using the following parameters $Z = 3 \text{ mm}$ and a 60% bandwidth.

frequency. The speed of sound in tissue is assumed to be constant at 1540 m/s. The PSF is simulated using a Gaussian-modulated cosine pulse with a wave number = 20.4 mm^{-1} (5-MHz center frequency), and a 0.2138-mm standard deviation (SD) unless stated otherwise. The scattering function consists of randomly distributed point scatterers with density of 40 scatterers/pulse-width, to simulate Gaussian statistics for the scatterer number. The PSF is convolved with the scattering function to obtain the precompression RF signal. The postcompression signals are generated after applying a uniform compression of the point scatterers (Céspedes 1993), and convolving the compressed point scatterers with the original PSF. The scattering function is bandlimited, as discussed in the theory for accurate estimation of the strain.

Spectral strain estimation is performed on the power spectra obtained by averaging 10 independent Fourier spectra obtained from an ensemble of A-lines (Welch 1967; Varghese 1995; Varghese and Donohue 1994). Frequency smoothing (Varghese 1995; Varghese and Donohue 1995) can also be used to generate the power spectra, which allows the use of a single pair of A-lines, similar to the strain estimation performed using the cross-correlation-based strain estimator. However, for the simulation results, we used the classical method of generating the power spectrum using independent uncorrelated data sets. Frequency smoothing is used later in this paper to generate the simulation and experimental elastograms. Frequency smoothing allows the use of a single pair of pre- and postcompression signals, providing a direct comparison between the elastograms generated using the coherent and incoherent methods.

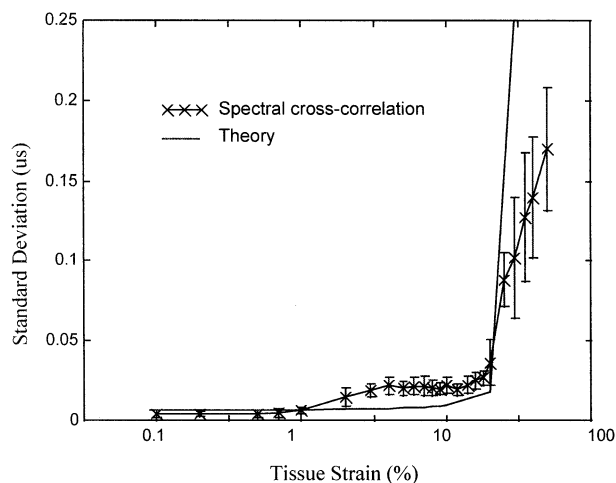


Fig. 5. Standard deviation of tissue strain estimates obtained using both simulation and theoretical results plotted as a function of strain. The theoretical and simulation results are obtained using the following parameters: $Z = 3$ mm; $B = 60\%$; $k_o = k_f = 20.4$ mm⁻¹.

Monte-Carlo simulations in MATLAB² were used to validate the theoretical results presented in the previous section. The spectral strain estimates were obtained over 25 sets of 10 independent realizations of the pre- and the postcompression RF signals. The corresponding SNR_e for each strain value is obtained using:

$$SNR_e = m_s / \sigma_s, \quad (14)$$

where m_s denotes the statistical mean strain estimate and σ_s denotes the SD for the strain noise obtained from the strain estimates.

Results

Figure 5 presents the SD of the spectral cross-correlation strain estimator using a 3-mm data segment, along with the theoretical result for a large range of applied strains. Note that the theoretical and simulation results follow the same trend, especially in the region where the SD increases rapidly with strain. The theoretical result forms the lower bound on the SD estimate, as illustrated in the figure.

The simulated SFs (Varghese and Ophir 1997; Varghese et al. 1998) obtained by plotting the SNR_e estimate corresponding to the tissue strain applied, addresses the limitations of the US system (such as time-bandwidth product, center frequency and sonographic SNR), as well as the signal processing algorithm are illustrated in Fig. 6 along with their corre-

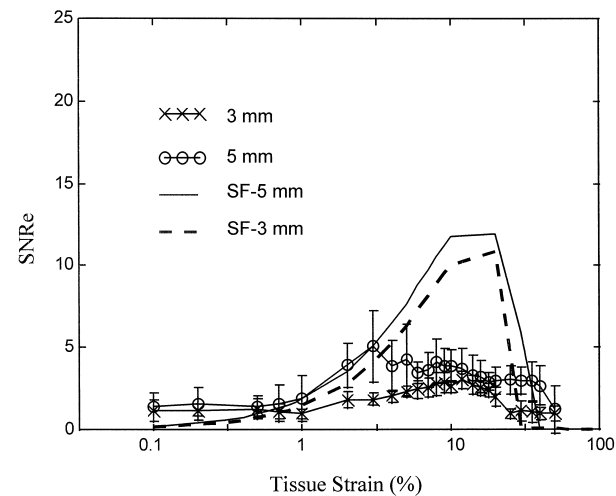


Fig. 6. Comparison of the theoretical and simulated SFs for the spectral cross-correlation strain estimator. The theoretical and simulation SFs were obtained using the following parameters $B = 60\%$; $k_o = k_f = 20.4$ mm⁻¹.

sponding theoretical SFs. Note that the simulation SFs follow the theoretical SFs at low strains, with the mean SNR_e dropping below the theoretical results. This large drop on the SNR_e is due to two factors: 1. the bias in the estimation of the spectral strain, which was previously discussed (Konofagou et al. 1999), and 2. the increased variance for large strains that is clearly observed in Fig. 5. Both these factors serve to reduce the SNR_e value obtained from the simulation result. The simulation SFs, however, illustrate the definite agreement with the theoretical SF among several elastographic parameters quantified using the SF, namely the sensitivity (the smallest value of the strain estimated accurately), saturation (the largest value of the strain estimated accurately) and in the dynamic range of strains estimated. Note also the improvement in the sensitivity and saturation values of the strain estimates with the use of the larger window length of 5 mm, which is also corroborated by the theoretical results.

Simulated SFs have been previously used to compare the noise performance between the coherent cross-correlation and centroid shift strain estimators (Konofagou et al. 1999). The robustness of the centroid shift strain estimation to axial jitter is also demonstrated, where the coherent cross-correlation method completely fails to estimate the strain incurred in tissue. Spectral cross-correlation also provides similar robustness to signal decorrelation (jitter, large applied strains etc), as does the spectral centroid shift algorithm. The robustness of the spectral algorithms is, therefore, primarily due to the use of the power spectrum.

² MATLAB is a registered trademark of The MathWorks, Inc.

SIMULATION AND EXPERIMENTAL ELASTOGRAMS

In this section, we present axial-strain elastograms obtained using both 1-D simulations using a finite element analysis (FEA) commercial software ALGOR (ALGOR, Inc., Pittsburgh, PA) and 3-D experimental phantom results. The comparison of the elastograms is made under the same conditions for all the imaging modalities shown.

Elastograms using simulated data

Methods. In this section, elastograms are generated for a simulated single inclusion phantom under uniform compression. We use the FEA software to estimate scatterer displacements under compression. The simulated incompressible and isotropic phantom contained a single inclusion 3 times stiffer than the homogeneous background (with a Young's modulus of 21 kPa). All the nodes in the simulated phantom are constrained to move solely in the axial direction (1-D motion model), thereby avoiding decorrelation due to motion in other directions.

A convolutional acoustic model that describes the interaction between the acoustic point-spread function (PSF) and the random scatterers present in the tissue supplement the 1-D tissue deformation model. This model allows incorporation of acoustic and signal-processing parameters; thus, allowing the generation of echo-signals (A-lines) obtained before and after a small applied compression. The ultrasonic PSF parameters used in the simulation are as follows: center frequency 5 MHz, 50% 6-dB bandwidth and 100 A-lines. A sampling frequency of 48 MHz was used to generate the RF A-lines.

The noise performance of the spectral estimators (centroid shift and spectral cross-correlation) are compared to the coherent cross-correlation-based strain estimator without global stretching (no correction for axial movement of the scatterers). The power spectrum for the spectral estimators is generated using a single pair of data segments ($Z = 3$ mm) using a 25-point frequency smoothing window (Varghese 1995; Varghese and Donohue 1995). Frequency smoothing (unlike time-averaging) of the Fourier spectrum allows the use of a single pair of pre- and postcompression RF signals to generate the elastogram similar to the case with the coherent cross-correlation-based strain estimator, without additional information.

Results. Figure 7 presents the elastograms obtained using both the coherent and incoherent methods, along with the ideal elastogram (*i.e.*, true strain image) for three different applied compressions. Note that, at the low strain value of 1% (Fig. 7, i), the elastogram gener-

ated using the cross-correlation algorithms (both coherent and incoherent) provides good correspondence to the ideal elastogram. The spectral cross-correlation provides the elastogram with the highest SNR_e when compared to all the other elastograms.

On the other hand, for larger applied strains (5% and 10%, Fig. 7, ii and iii), the coherent cross-correlation algorithm fails to accurately estimate tissue strain due to the increased signal decorrelation errors (Fig. 7b, ii & iii, respectively). In fact, at 5% applied compression, the inclusion is still visible, being 3 times harder than the background and, thus, experiencing a much lower strain, allowing it to be depicted with a good signal-to-noise ratio (Konofagou *et al.* 1999). However, we have to point out that, without *a priori* knowledge of the position of the inclusion, the lesion position could easily be misregistered in Fig. 7b, ii. On the other hand, the elastogram generated using the spectral methods at 5% and 10% compression (Fig. 7c, ii & iii, respectively) illustrates the robustness associated with the spectral methods.

Note that spectral cross-correlation provides the elastogram with the closest correspondence to the ideal elastogram in all the cases illustrated in this paper. Spectral cross-correlation, therefore, provides all the advantages offered by the spectral centroid shift method (direct, incoherent and robust strain estimation), in addition to providing precise strain estimates. In the next section, we present elastograms obtained using an elastographic experimental phantom. The experimental results provide a complete 3-D situation where axial, lateral and elevational signal decorrelation are present, unlike the 1-D situation illustrated in this section.

Elastograms using experimental data

Methods. The ultrasound system used for elastography is a Diasonics Spectra II real-time scanner (Diasonics Inc., Santa Clara, CA) operating with dynamic receive focusing and a single transmit focus. The transducer used was a 7.5 MHz linear array (40 mm) with a 60% bandwidth. The digitizer used is an 8-bit digitizer (LeCroy Corp., Spring Valley, NY) with a sampling rate of 48 MHz. The system also includes a motion control system, and a compression device. A personal computer controls the operation of the entire system. A complete description of the elastography system is presented by Céspedes (1993). A gelatin phantom³ ($90 \times 90 \times 90$ mm³) containing a cylindrical inclusion with a 20-mm diameter, positioned at the center of the phantom and 3 times stiffer than the background, was used to compare the performance of the strain estimators.

³ The elastographic phantom was supplied courtesy of Dr. Timothy Hall (Hall *et al.* 1997).

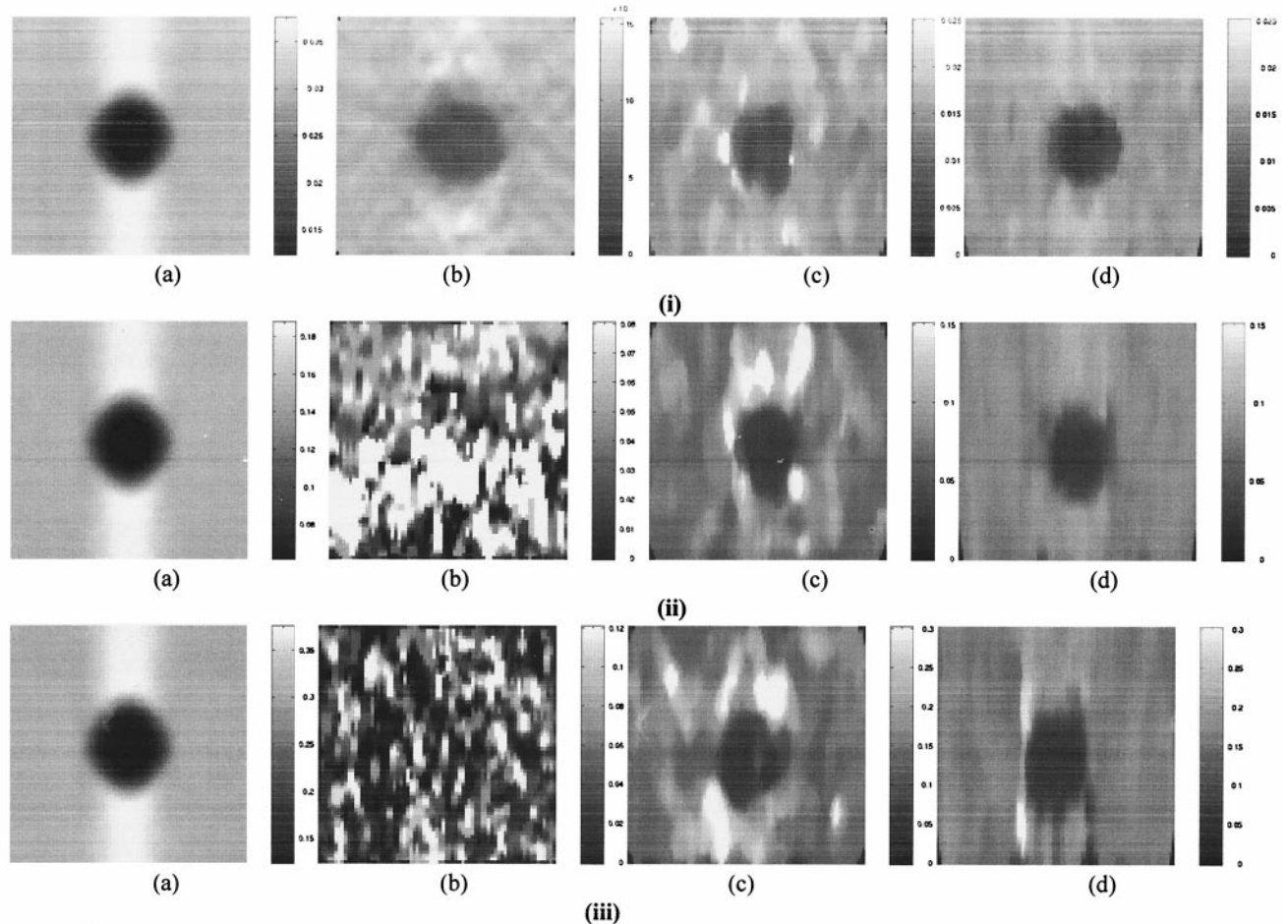


Fig. 7. Elastograms obtained using the 1-D model for scatterer motion using the FEA simulation model for (i) 1%, (ii) 5% and (iii) 10% applied compression using a 3-mm window. The simulated phantom contains an inclusion that is 3 times stiffer than the background. (a) Ideal elastogram; (b) elastogram obtained using the coherent cross-correlation method; (c) elastogram obtained using the spectral centroid method; (d) elastogram obtained using spectral cross-correlation of the power spectra.

The phantom contains scatterers (graphite flakes) and is used to obtain RF scans before and after the externally applied uniform compression. A large compressor is used to simulate uniform stress conditions in the phantom. The phantom is lubricated on the top and bottom surfaces with corn oil to simulate slip boundary conditions and is free on both lateral and elevational sides.

Results. Comparison of the estimation performance using coherent cross-correlation and spectral strain estimators is illustrated qualitatively using elastograms obtained at both low (0.5%) and high (3%) applied strains in Fig. 8. Note that, similarly to the simulation results, the cross-correlation strain estimation (coherent and incoherent) provides the elastogram with the highest SNR_e for the low compression of 0.5% (Fig. 8, i), when compared to the centroid shift

method. However, for the large applied compression of 3% (Fig. 8, ii) the coherent strain estimator fails completely when compared to the spectral methods, which produce a reasonable elastogram. The incoherent spectral correlation algorithm, however, produces the elastogram with the higher SNR_e among the spectral methods. Averaging several elastograms obtained from independent pre- and postcompression data can be used to further improve the elastograms for the spectral methods. However, averaging is not useful for the coherent cross-correlation strain estimator in this case because the RF signals are completely decorrelated, producing only noise (Fig. 8a, ii).

Two major differences can be observed between the 1-D simulation results and the experimental results: 1. the mechanical artefacts for the 1-D simulation elastograms are along the top and bottom axes of

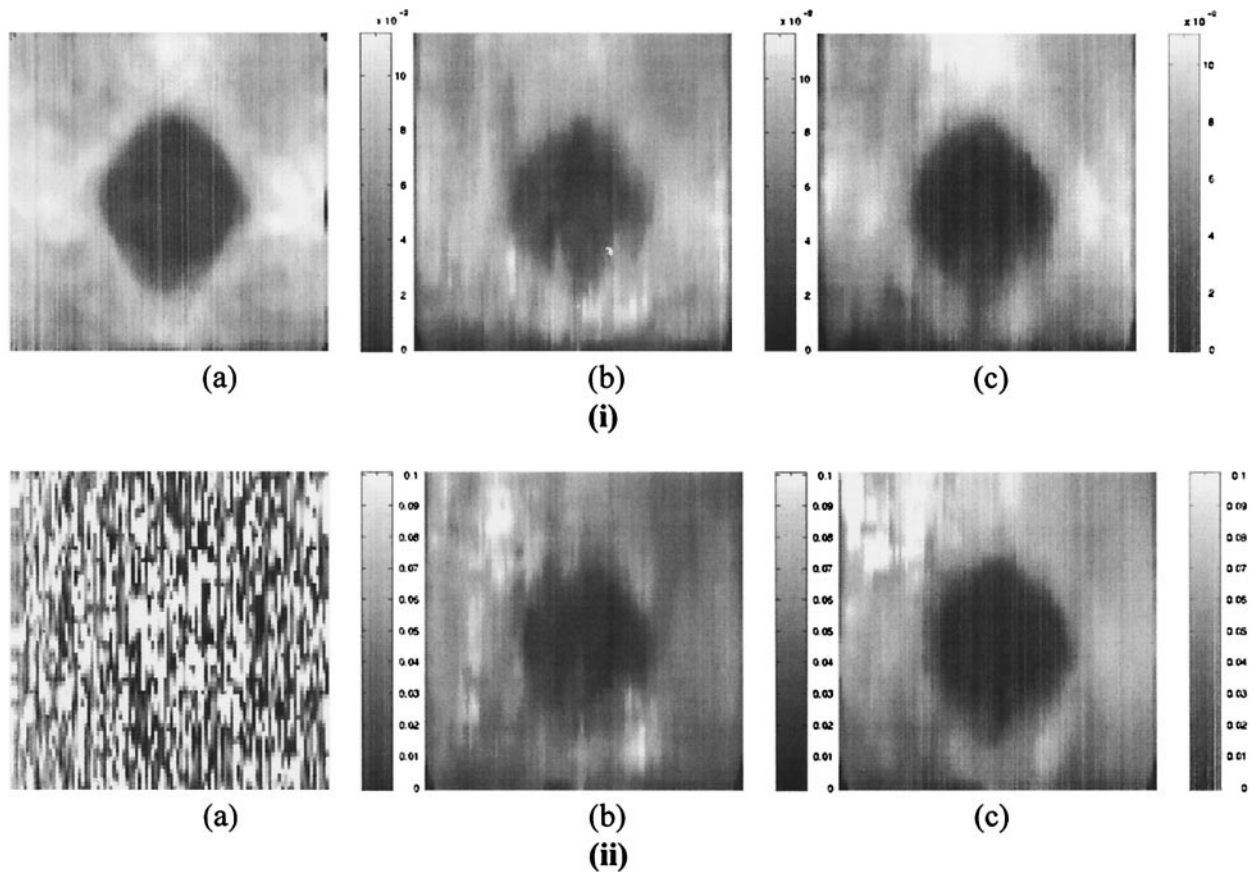


Fig. 8. Elastograms obtained using coherent and incoherent strain estimation algorithms, for a phantom with a inclusion that is 3 times stiffer than the background. The RF signals are obtained using a 7.5-MHz linear array with a 50% bandwidth. The elastograms are obtained using a (i) 0.5% and (ii) 3% applied compression using a 3-mm window. (a) Elastogram obtained using the coherent cross-correlation method; (b) elastogram obtained using centroid strain estimation; (c) elastogram obtained using spectral cross-correlation of the power spectra.

the inclusion, when compared to the more complicated artefacts observed for the 3-D case; and 2. the cross-correlation algorithm fails at relatively lower applied strains (3% instead of 5% or 10%) than in the simulation results, due to lateral and elevational decorrelation involved in the 3-D model. The spectral methods yield similar results in both cases of low and high applied strains, demonstrating its robustness in a 3-D scenario, as well.

CONCLUSIONS

In this paper, we present a new spectral cross-correlation strain estimator. Spectral cross-correlation is shown to be more sensitive to small shifts in the power spectrum and, thus, provides better estimation for small strains when compared to the spectral centroid shift. In addition to possessing the advantages of the spectral centroid shift estimator, spectral cross-correlation pro-

vides precise strain estimation even at low tissue strains and higher SNR_e values. The improvement in the SNR_e and sensitivity is illustrated in the theoretical SF plots, and in both the simulated and experimental elastograms.

The robustness and noise performance of both the spectral estimators have been quantified in terms of their strain estimation variance and SF analysis in this paper. Theoretical expressions for the variance are derived for both the spectral cross-correlation and spectral centroid shift algorithms. The spectral SFs illustrate that the range of strains estimated accurately using this approach lie in the region where the coherent cross-correlation estimator fails completely. This realization also leads to the possibility of combining the coherent cross-correlation method with the spectral cross-correlation approach to increase the dynamic range of strains estimated.

Spectral cross-correlation provides a robust (noise-

resistant) and motion-invariant method (Konofagou et al. 1999) of estimating strain, which can be extremely beneficial in cases with large signal decorrelation errors. Comparison of the simulated and experimental elastograms illustrates that the spectral cross-correlation method produces the best elastograms, both at high and low applied strains. The spectral cross-correlation algorithm may be particularly useful for obtaining elastograms in noisy environments, such as in a hand-held elastography setup, or in environments with undesired scatterer motion, like intravascular elastography. The spectral estimators provide a means for the implementation of elastography in regions that have hitherto been impossible to image.

Acknowledgements—This work is supported in part by NIH Program Project grant P01-CA64597 awarded to the University of Texas.

REFERENCES

- Alam SK, Ophir J, Konofagou EE. An adaptive strain estimator for elastography. *IEEE Trans Ultrason Ferroel Freq Cont* 1998;45(2):461–472.
- Alam SK, Ophir J, Varghese T. Elastographic axial resolution criteria: An experimental study. *IEEE Trans Ultrason Ferroel Freq Cont* 2000;47(1):304–309.
- Bahr RK, Bucklew JA, Flax SW. Optimal center frequency estimation for backscattered ultrasound pulses. *IEEE Trans Son Ultrason* 1985;32(6):809–814.
- Bertrand M, Meunier M, Doucet M, Ferland G. Ultrasonic biomechanical strain gauge based on speckle tracking. *Proc 1989 IEEE Ultrason Symp* 1989;2:859–864.
- Bilgen M, Insana MF. Deformation models and correlation analysis in elastography. *J Acoust Soc Am* 1996;99:3212–3224.
- Céspedes EI. Elastography: Imaging of biological tissue elasticity. Ph.D. Dissertation, University of Houston, 1993.
- Fellingham LL, Sommer PG. Ultrasonic characterization of tissue structure in the in vivo human liver and spleen. *IEEE Trans Sonics Ultrason* 1984;31:418–428.
- Hall TJ, Bilgen M, Insana MF, Krouskop TA. Phantom materials for elastography. *IEEE Trans Ultrason Ferroelec Freq Cont* 1997;44:1355–1365.
- Insana MF, Wagner RF, Brown DG, Hall TJ. Describing small-scale structure in random media using pulse-echo ultrasound. *J Acoust Soc Am* 1990;87:179–192.
- Kay SM. *Fundamentals of statistical signal processing: Estimation theory*. New York: Prentice Hall, 1996.
- Konofagou EE, Varghese T, Ophir J, Alam SK. Power spectral strain estimators in elastography. *Ultrasound Med Biol* 1999;25(7):1115–1129.
- Krouskop TA, Vinson S, Goode B, Dougherty D. A pulsed Doppler ultrasonic system for making noninvasive measurements of the mechanical properties of soft tissue. *J Rehab Res Dev* 1987;24:1–8.
- Kuc R, Haghkerder K, O'Donnell M. Presence of cepstral peaks in random reflected ultrasound signal. *Ultrasonic Imaging* 1986;8:196–212.
- Landini L, Verrazzani L. Spectral characterization of tissue microstructure by ultrasound: A stochastic approach. *IEEE Trans Ultrason Ferroel Freq Cont* 1990;37:448–456.
- Lizzi FL, Ostromogilsky M, Feleppa EJ, Rorke MC, Yaremko MM. Relationship of ultrasonic spectral parameters to features of tissue microstructure. *IEEE Trans Ultrason Ferroel Freq Cont* 1987;33(3):319–329.
- O'Donnell M, Skovoroda AR, Shapo BM. Measurement of arterial wall motion using Fourier based speckle tracking algorithms. *Proc 1991 IEEE Ultras Symp* 1991;2:1101–1104.
- O'Donnell M, Skovoroda AR, Shapo BM, Emelianov SY. Internal displacement and strain imaging using ultrasonic speckle tracking. *IEEE Trans Ultrason Ferroel Freq Cont* 1994;41:314–325.
- Ophir J, Céspedes EI, Ponnekanti H, Yazdi Y, Li X. Elastography: a quantitative method for imaging the elasticity of biological tissues. *Ultrasonic Imaging* 1991;13:111–134.
- Ophir J, Kallel F, Varghese T, Bertrand M, Céspedes I, Ponnekanti H. Elastography: A systems approach. *Int J Imaging Syst Technol* 1997;8:89–103.
- Papoulis A. *Probability random variables and stochastic processes*. New York: McGraw Hill, 1984.
- Parker KJ, Huang SR, Musulin RA, Lerner RM. Tissue response to mechanical vibrations for sonoelasticity imaging. *Ultrasound Med Biol* 1990;16:241–246.
- Talhami HE, Wilson LS, Neale ML. Spectral tissue strain: A new technique for imaging tissue strain using intravascular ultrasound. *Ultrasound Med Biol* 1994;20(8):759–772.
- Varghese T. Spectral redundancy in tissue characterization. Ph.D. Dissertation, University of Kentucky, 1995.
- Varghese T, Ophir J. Characterization of elastographic noise using the envelope of echo signals. *Ultrasound Med Biol* 1998;24(4):543–555.
- Varghese T. Spectral redundancy in tissue characterization. Ph.D. Dissertation, University of Kentucky, 1995.
- Varghese T, Ophir J. A theoretical framework for performance characterization of elastography: The strain filter. *IEEE Trans Ultrason Ferroel Freq Cont* 1997;44(1):164–172.
- Varghese T, Bilgen M, Ophir J. Multiresolution imaging in elastography. *IEEE Trans Ultrason Ferroel Freq Cont* 1998;45(1):65–75.
- Varghese T, Konofagou E, Ophir J, Alam SK. Coherent vs. incoherent strain estimation in elastography. AIUM conference, San Antonio, Texas, March 14–17, 1999.
- Varghese T, Donohue KD. Mean scatterer spacing estimates with spectral correlation. *J Acoust Soc Am* 1994;96:3504–3515.
- Varghese T, Donohue KD. Estimating mean scatterer spacing estimates with the frequency-smoothed spectral autocorrelation function. *IEEE Trans Ultrason Ferroel Freq Cont* 1995;42(3):451–463.
- Walker FW, Trahey EG. A fundamental limit on delay estimation using partially correlated speckle signals. *IEEE Trans Ultrason Ferroel Freq Cont* 1995;42:301–308.
- Weinstein E, Weiss A. Fundamental limitations in passive time-delay estimation Part II: Wide-band systems. *IEEE Trans Acoust Speech Sig Proc* 1984;31:1064–1078.
- Welch PD. The use of fast Fourier transforms for the estimation of power spectra: A method based on time averaging over short modified periodograms. *IEEE Trans Audio Electroacoust* 1967;15:70–73.
- Wilson LS, Robinson DE. Ultrasonic measurement of small displacements and deformations of tissue. *Ultrasonic Imag* 1982;4:71–82.
- Yamakoshi Y, Sato J, Sato T. Ultrasonic imaging of internal vibration of soft tissue under forced vibration. *IEEE Trans Ultrason Ferroel Freq Cont* 1990;37(2):45–53.

APPENDIX A

Strain estimation using spectral cross-correlation

The cross-correlation function between the pre- and the postcompression power spectra illustrated in eqn (7) is written as:

$$S(k_0) = \int_{-\infty}^{\infty} R_1(k + k_0) R_2(k) dk, \quad (\text{A-1})$$

where k_0 denotes the spectral shift. Substituting eqn (6) into eqn (A-1) and simplifying, we obtain:

$$S(k_0) = \frac{1}{16a} \int_{-\infty}^{\infty} \exp \left[-\frac{1}{2} \left(\frac{((k+k_0-k_h)^2 L_h^2 + (k+k_0-k_e)^2 L_e^2)}{(k-k_h)^2 L_h^2 + (k-ak_e)^2 \frac{L_e^2}{a^2}} \right) \right] dk. \quad (\text{A-2})$$

Rearranging the terms leads to:

$$S(k_0) = \frac{\delta}{16a} \int_{-\infty}^{\infty} \exp \left[-\frac{(2L_h^2 + L_e^2(1+1/\alpha^2))}{2} \left(k - \frac{(2k_h - k_0)L_h^2 + (k_e(1+1/\alpha) - k_0)L_e^2}{2L_h^2 + L_e^2(1+1/\alpha^2)} \right)^2 \right] dk, \quad (\text{A-3})$$

where

$$\delta = \exp \left[-\frac{1}{2} \left(\frac{((2k_h - k_0)L_h^2 + (k_e(1+1/\alpha) - k_0)L_e^2)^2}{2L_h^2 + L_e^2(1+1/\alpha^2)} + (k_o^2 + 2k_h^2 - 2k_0k_h)L_h^2 + (k_o^2 + 2k_e^2 - 2k_0k_e)L_e^2 \right) \right]. \quad (\text{A-4})$$

Equation (A-3) is of the form

$$\int_{-\infty}^{\infty} \exp(-ax^2) dx = \sqrt{\pi/\alpha}, \text{ substituting, we obtain:}$$

$$S(k_0) = \frac{1}{16a} \delta \sqrt{\frac{2\pi}{(2L_h^2 + L_e^2(1+1/\alpha^2))}}. \quad (\text{A-5})$$

To find the spectral shift, which occurs at the maximum of the cross-correlation, we equate the derivative of $S(k_0)$ with respect to k_0 to zero:

$$\frac{dS(k_0)}{dk_0} = 0, \quad (\text{A-6})$$

or

$$\left(\frac{1}{16a} \delta \sqrt{\frac{2\pi}{(2L_h^2 + L_e^2(1+1/\alpha^2))}} \right) \times \left(-\frac{1}{2} \left(\frac{2((2k_h - k_0)L_h^2 + (k_e(1+1/\alpha) - k_0)L_e^2)(L_h^2 + L_e^2)}{2L_h^2 + L_e^2(1+1/\alpha^2)} + (2k_o - 2k_h)L_h^2 + (2k_o - 2k_e)L_e^2 \right) \right) = 0, \quad (\text{A-7})$$

that is

$$\left(\frac{2((2k_h - k_0)L_h^2 + (k_e(1+1/\alpha) - k_0)L_e^2)(L_h^2 + L_e^2)}{2L_h^2 + L_e^2(1+1/\alpha^2)} + (2k_o - 2k_h)L_h^2 + (2k_o - 2k_e)L_e^2 \right) = 0. \quad (\text{A-8})$$

Substituting for $\alpha = 1/(1-s)$, we obtain:

$$\left(\frac{2((2k_h - k_0)L_h^2 + (k_e(2-s) - k_0)L_e^2)(L_h^2 + L_e^2)}{(2L_h^2 + L_e^2(2-2s+s^2))((2k_o - 2k_h)L_h^2 + (2k_o - 2k_e)L_e^2)} \right) = 0. \quad (\text{A-9})$$

In eqn (A-9), neglecting s^2 , because s^2 is much smaller than s , eqn (A-9) reduces to:

$$(2k_h L_h^2 + k_e(2-s)L_e^2 - k_0(L_h^2 + L_e^2))(L_h^2 + L_e^2) + 2(L_h^2 + L_e^2(1-s)) \times (-k_h L_h^2 - k_e L_e^2 + k_0(L_h^2 + L_e^2)) = 0. \quad (\text{A-10})$$

Collecting all the terms with k_o , we obtain:

$$k_o = \frac{-sL_e^2(k_e L_e^2 - k_e L_h^2 + 2k_h L_h^2)}{(L_h^2 + L_e^2)(L_h^2 + L_e^2 - 2sL_e^2)}. \quad (\text{A-11})$$

Making the assumption that both the pulse and scattering function have the same spatial center frequency (*i.e.*, $k_e \cong k_h$), we have:

$$k_o = \frac{-sk_h L_e^2}{(L_h^2 + L_e^2 - 2sL_e^2)}. \quad (\text{A-12})$$

Because the spectrum of the backscattered signal is determined by the signal (PSF or scattering spectrum) with the smallest bandwidth, we have $L_h \cong L_e$, leading to:

$$k_o = \frac{-sk_h}{2(1-s)} \approx \frac{-k_h}{2} s(1+s) \approx -\frac{k_h}{2} s. \quad (\text{A-13})$$

We obtain eqn (A-13) by neglecting s^2 , because s^2 is much smaller than s . The spectral shift in the pre- and postcompression spectra, therefore, gives the tissue strain scaled by the center frequency of the PSF.

APPENDIX B

Expression for the spectral correlation coefficient

With the signal model presented in eqn (6), we first derive the cross-correlation function between the pre- and postcompression power spectrum obtained from windowed signals, as:

$$\langle \hat{\Gamma}_{12}(k) \rangle = \left\langle \frac{1}{Z} \int_{-1/2}^{1/2} R_1(\tau - k) R_2(\tau) d\tau \right\rangle, \quad (\text{B-1})$$

where the bracket $\langle \rangle$ denotes the ensemble average, and k denotes the shift variable. The autocorrelation functions $\hat{\Gamma}_{11}(k)$ for the pre- and $\hat{\Gamma}_{22}(k)$ for the postcompression power spectrum are also computed. The effective spectral correlation coefficient can be written as:

$$\rho = \frac{\hat{\Gamma}_{12}(0)}{\sqrt{\hat{\Gamma}_{11}(0)\hat{\Gamma}_{22}(0)}} = \rho_0 \times M, \quad (\text{B-2})$$

where

$$\hat{\Gamma}_{12}(0) = \frac{1}{16\alpha} \frac{\sqrt{2}}{\eta} \exp\left(-\tau^2 + \frac{2\zeta^2}{\eta^2}\right), \quad (\text{B-3})$$

$$\hat{\Gamma}_{11}(0) = \frac{1}{16} \frac{1}{\sqrt{L_j^2 + L_h^2}} \exp\left(-\tau^2 + \frac{(k_j L_j^2 + k_h L_h^2)^2}{L_j^2 + L_h^2}\right), \quad (\text{B-4})$$

and

$$\hat{\Gamma}_{22}(0) = \frac{1}{16\alpha^2} \frac{1}{\sqrt{L_j^2 + (L_h/\alpha)^2}} \exp\left(-\tau^2 + \frac{(k_j L_j^2 + k_h L_h^2/\alpha^2)}{L_j^2 + (L_h/\alpha)^2}\right), \quad (\text{B-5})$$

where

$$\eta^2 = 2L_j^2 + \left(1 + \frac{1}{a^2}\right)L_h^2, \quad (\text{B-6})$$

$$\zeta = k_j L_j^2 + \frac{1}{2} \left(1 + \frac{1}{a}\right) k_h L_h^2, \quad (\text{B-7})$$

$$\tau^2 = (k_j L_j)^2 + (k_h L_h)^2. \quad (\text{B-8})$$

Substituting, we obtain the expression for ρ_0 , as follows:

$$\rho_0 = \frac{\sqrt{2}(L_j^2 + (L_h/\alpha)^2)^{1/4} (L_j^2 + L_h^2)^{1/4}}{\eta} \exp\left(\frac{2\zeta^2}{\eta^2} - \frac{1}{2} \left(\frac{(k_j L_j^2 + k_h L_h^2)^2}{L_j^2 + L_h^2} + \frac{(k_j L_j^2 + k_h L_h^2/\alpha^2)^2}{L_j^2 + (L_h/\alpha)^2}\right)\right). \quad (\text{B-9})$$

The term ρ_0 represents the peak spectral correlation coefficient. The factor M in eqn (B-2) is due to the finiteness of the window length and is given by the integral:

$$M = \frac{1}{Z} \int_{-Z/2}^{Z/2} \exp\left(-z \left((k_j L_j^2 + k_h L_h^2) - \frac{2\zeta(L_j^2 + L_h^2)}{\eta^2}\right)\right) \exp\left(-z^2 \left(\frac{(L_j^2 + L_h^2)}{2} - \frac{(L_j^2 + L_h^2)}{2\eta^2} - \frac{\eta^2}{8}\right)\right) dz. \quad (\text{B-10})$$

For zero strain $s = 0$, $a = 1$ and $M = 1$. Non-zero strain, on the other hand, yields $M < 1$ and, consequently, reduces the spectral correlation coefficient ρ . The expression for the spectral correlation coefficient, eqn (B-2), is substituted into eqn (9) to obtain the CRLB on the variance of the spectral cross-correlation strain estimator.

APPENDIX C

CRLB bound on the power spectral variance

The CRLB on variance of the total power for a WSS Gaussian power spectrum (Bahr et al. 1985; Kay 1996) is given by the expression:

$$\sigma_{\text{PSD}}^2(P_o)_{\text{CRLB}} \geq \frac{1}{Z \int_{-1/2}^{1/2} \left(\frac{\partial \ln P(k)}{\partial k}\right)^2 dk}, \quad (\text{C-1})$$

where

$$P(k) = P_o R(k) + \beta^2$$

is the power spectrum, where $\int_{-1/2}^{1/2} R(k) dk = 1$, for a Gaussian random process. This expression reduces to:

$$\sigma_{\text{PSD}}^2(P_o)_{\text{CRLB}} \geq \frac{1}{Z \int_{-1/2}^{1/2} \left(\frac{\partial R(k)/\partial k}{R(k) + \beta^2}\right)^2 dk}. \quad (\text{C-2})$$

Substituting the precompression signal from eqn (6), into eqn (C-2), we obtain:

$$\sigma_{\text{PSD}}^2(P_o)_{\text{CRLB}} \geq \frac{1}{Z \int_{-1/2}^{1/2} \left(\frac{k(L_h^2 + L_j^2)R(k)}{R(k) + 1/SNR^2}\right)^2 dk}. \quad (\text{C-3})$$

Note that this expression is very similar to the CRLB expression obtained for the variance of the centroid or center frequency estimator, eqn (D-4). The variance of the power spectral estimate will change with applied strain (use of the postcompression signal in eqn (C-2)) due to the presence of the strain α and SNR terms.

APPENDIX D

Variance of the centroid strain estimator

Axial strain (s) is estimated from the spectral upshift (Konofagou et al. 1999) in the center frequency between the power spectrum of the post- and precompression A-lines, viz:

$$\hat{s} = \frac{\hat{k}_{c2} - \hat{k}_{c1}}{\hat{k}_{c1}} = \frac{\hat{k}_{c2}}{\hat{k}_{c1}} - 1, \quad (\text{D-1})$$

where \hat{k}_{c2} and \hat{k}_{c1} are the center frequency estimates from the pre- and postcompression signals, respectively, for a data window with duration Z . The variance of the strain estimate, therefore, depends on the variance of the center frequency (centroid) estimates.

The CRLB on variance of the centroid estimate has been computed for a WSS Gaussian power spectrum (Bahr et al. 1985; Kay 1996), and is given by:

$$\sigma_c^2(\hat{k}_c)_{\text{CRLB}} \geq \frac{1}{Z \int_{-1/2}^{1/2} \left(\frac{\partial \ln P(k; k_c)}{\partial k_c}\right)^2 dk}, \quad (\text{D-2})$$

where $P(k; k_c)$ is the power spectrum and k_c is the center frequency of a Gaussian random process. This expression reduces to:

$$\sigma_c^2(\hat{k}_c)_{\text{CRLB}} \geq \frac{1}{Z \int_{-1/2}^{1/2} \left(\frac{\partial R(k)/\partial k}{R(k) + \beta^2}\right)^2 dk}, \quad (\text{D-3})$$

where $R(k)$ represents either the pre- or postcompression power spectral density signals, and β represents a percentage of the additive noise level. Equation (D-3) can be written as:

$$\sigma_c^2(\hat{k}_c)_{\text{CRLB}} \geq \frac{1}{Z \int_{-1/2}^{1/2} \left(\frac{k(L_h^2 + L_j^2)R(k)}{R(k) + 1/SNR^2}\right)^2 dk}. \quad (\text{D-4})$$

Equation (D-4) has to be evaluated numerically to generate an estimate of the variance of the centroid estimate.

The variance of the strain estimate depends on the ratio of two random variables, as illustrated in eqn (D-1). Assuming a Gaussian distribution of the random variables, the ratio of two random variables

is described by a Cauchy's distribution (Papoulis 1984). The moments of a Cauchy distribution are not defined because the integral does not converge. Therefore, to obtain a theoretical estimate of the variance, we replace the term in the denominator of eqn (D-1) by the known constant center frequency of the process. The denominator in eqn (D-1) now represents a normalization of the center frequency estimates of the pre- and postcompression signals. This substitution will introduce a bias in the strain estimate due to changes in the center frequency estimate with attenuation. Equation (D-1) can be rewritten as:

$$\hat{s} = \frac{\hat{k}_{c2} - \hat{k}_{c1}}{k_c}. \quad (\text{D-5})$$

The variance of the strain estimate can now be written as:

$$\sigma_s^2(\hat{s})_{\text{CRLB}} \geq \frac{1}{k_c^2} [\sigma_c^2(\hat{k}_{c1}) + \sigma_c^2(\hat{k}_{c2}) - 2\text{Cov}(\hat{k}_{c1}, \hat{k}_{c2})]. \quad (\text{D-6})$$

Equation (D-6) reduces to:

$$\sigma_s^2(\hat{s})_{\text{CRLB}} \geq \frac{1}{k_c^2} [\sigma_c^2(\hat{k}_{c1}) + \sigma_c^2(\hat{k}_{c2}) - 2\rho\sigma_c(\hat{k}_{c1})\sigma_c(\hat{k}_{c2})], \quad (\text{D-7})$$

where ρ is the correlation coefficient between the center frequency estimates. If the center frequency estimates are uncorrelated, eqn (D-7) reduces to:

$$\sigma_s^2(\hat{s})_{\text{CRLB}} \geq \frac{1}{k_c^2} [\sigma_c^2(\hat{k}_{c1}) + \sigma_c^2(\hat{k}_{c2})]. \quad (\text{D-8})$$

The variance of the center frequency estimate obtained from the precompression power spectrum depends only on the sonographic SNR. However, the variance of the center frequency estimate obtained from the strained postcompression power spectrum depends on the increased variance due to signal decorrelation (causing the frequency upshift and spreading of the power spectrum). The reduction in the SNR_s with strain is determined from the reduction in the spectral correlation coefficient between the pre- and postcompression power spectrum.